JOURNAL OF MATERIALS SCIENCE 25 (1990) 5055–5062

Electron microscopy of heavy metal waste in cement matrices

D. G. IVEY, R. B. HEIMANN*
*Department of Mining, Metallurgical and Petroleum Engineering, University of Alberta, Edmonton, Alberta, Canada T69 2G6, * and also Materials and Testing Department, Alberta Research Council, Edmonton, Alberta, Canada T6H 5X2*

M. NEUWIRTH, S. SHUMBORSKI, D. CONRAD
Alberta Environmental Centre, Vegreville, Alberta, Canada T0B 4L0

R. J. MIKULA, W. W. LAM
Fuel Processing Laboratory, Energy, Mines and Resources, Canada, CANMET, Devon, Alberta, Canada T0C 1E0

Ordinary Portland cements mixed with various amounts of chromium metal in the form of nitrates ($Cr(NO_3)_3$), to simulate industrial waste, have been studied by electron microscopy techniques, i.e. scanning electron and scanning transmission electron microscopy. Trivalent chromium was found to be chemically incorporated in all hydrated cement phases, and appeared to substitute for silicon in calcium silicate hydrate (C–S–H), which is the major product of hydration. Chromium was also concentrated in polycrystalline Ca–Cr-rich phases.

1. Introduction

Industrial wastes, containing heavy metals such as lead, chromium, mercury, vanadium, zinc and cadmium, can be disposed of by incorporation into cement matrices, by means of solidification/stabilization processes [1–3]. However, very little is known about the distribution and stability of these contaminants within cement matrices. Electron microscopy techniques, i.e. scanning electron and scanning transmission electron microscopy (SEM and TEM/STEM), can be quite useful in studying the complex microstructures associated with these cements. SEM and TEM/STEM are complementary techniques in the sense that SEM provides relatively large-scale microstructural and compositional information ($\approx 1\,\mu m$), while TEM/STEM gives much higher resolution or more localized information (< 1 nm). Morphological changes in cement associated with the addition of a particular waste, as well as the location of contaminants within the various cement phases, can therefore be monitored through various imaging, electron diffraction and X-ray spectroscopy techniques associated with SEM and TEM/STEM. This information can ultimately lead to a better understanding of the stabilization mechanisms.

Detailed TEM/STEM analysis of cement-stabilized waste material has up to now been virtually non-existent, primarily due to the difficulty in preparing electron-transparent specimens (≈ 100 nm thick) from cementitious materials. However, as reported here, adequate specimens can be prepared, in a relatively short period of time, by a combined mechanical dimpling/ion-milling process.

In the present study, cements mixed with various amounts of chromium metal in the form of nitrates, to simulate industrial waste, were investigated. Chromium was chosen for several reasons. It is generally only a very low-level contaminant in Portland cement (< 50 p.p.m.), and it has a characteristic K_α X-ray peak which is sufficiently isolated from any X-ray peaks generated by other cement constituents. Both of these features help to facilitate identification of the metal species. Also, chromium is known to accelerate the hydration reaction and strength development in cement [4, 5], which may be of practical benefit. The effect of leaching on these specimens will be reported at a later date.

2. Experimental procedure

Samples of ASTM Type 10 or ordinary Portland cement (OPC) (Table I) were mixed with 0.1M, 0.4M and 1.0M solutions of $Cr(NO_3)_3 \cdot 9H_2O$, at a solution/cement ratio of 0.33. The 0.1M sample had a concentration similar to actual industrial wastes. The higher concentrations were also studied for two reasons: (1) to enhance our chances of finding chromium in the hydrated pastes, especially in the TEM/STEM analysis, and (2) to determine concentration effects on the containment mechanisms. A control

TABLE I Typical compound composition of OPC

Compound	wt %
Tricalcium silicate C_3S	55
Dicalcium silicate C_2S	20
Tricalcium aluminate C_3A	12
Tetracalcium aluminoferrite C_4AF	9
Gypsum $C\bar{S}H_2$	3.5

0022–2461/90 $03.00 + .12

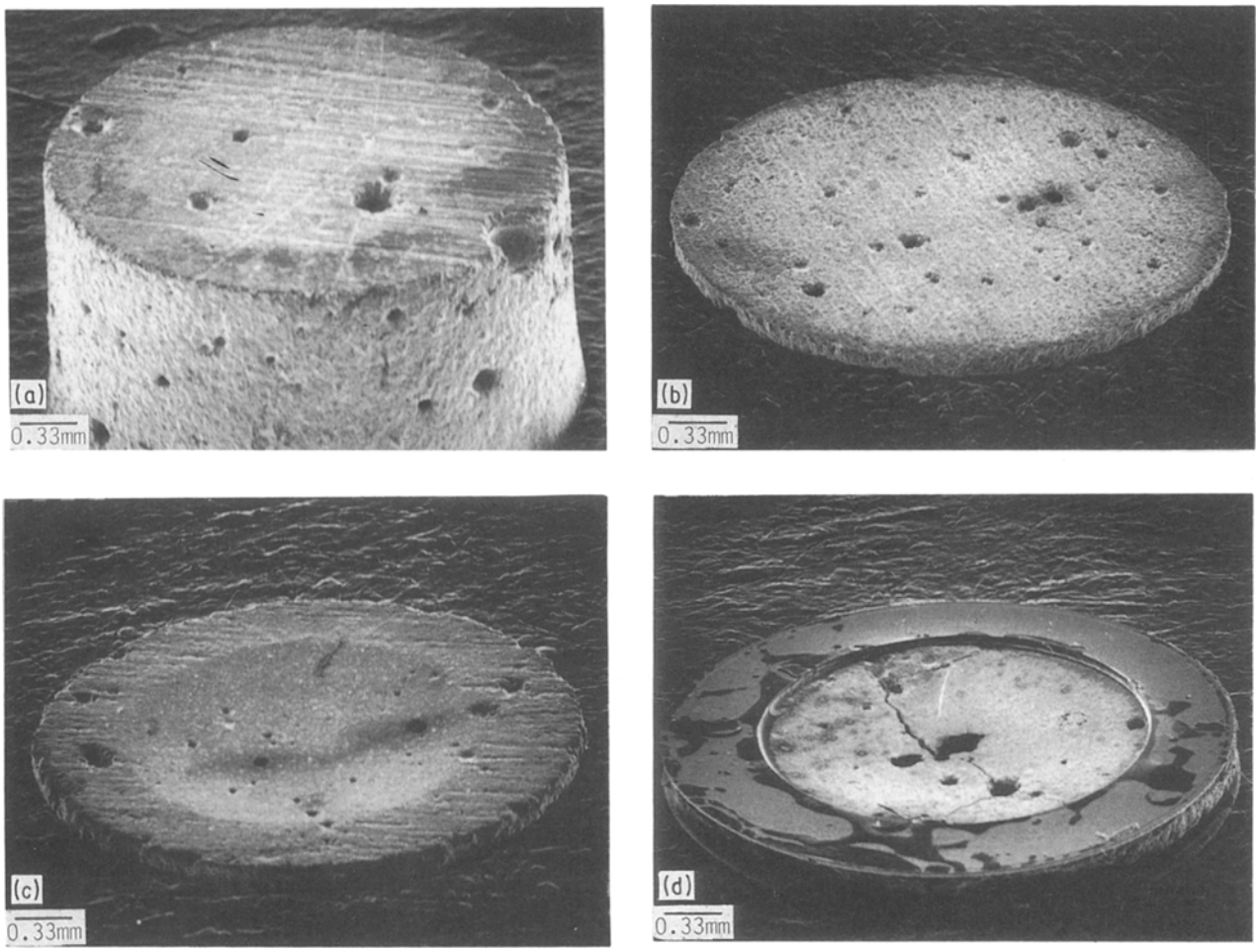

Figure 1 Scanning electron micrographs depicting the sequence of TEM specimen preparation. See text for details.

sample, i.e. OPC mixed with distilled water with the same solution/cement ratio was also fabricated. The samples were mixed and cast in cylindrical moulds, 45 mm i.d. by 75 mm high. Samples (500 to 600 g weight) were cured at 96% r.h. for 36 d at 25°C.

Both leached and unleached specimens were analysed by X-ray diffraction, in a Rigaku RU-200B X-ray diffractometer, prior to electron microscopy analysis. SEM analysis was done with a Hitachi X-650 SEM equipped with an energy dispersive spectrometer (Tracor 30 mm^3 Si (Li) detector) as well as with a JEOL 840A in conjunction with a Tracor Northern 5500 X-ray spectrometer. The incident beam current was approximately 0.2 nA at 25 keV unless otherwise specified. Specimens for SEM were prepared by fracturing the cured specimens in air and then coating a relatively flat surface with a thin conducting layer to prevent charging effects. Carbon was used to coat these samples, even though gold coatings are generally better for producing high-quality micrographs. Gold tends to absorb X-rays to a much larger degree than carbon, reducing the efficiency of X-ray collection. This is a particular problem for lighter elements such as silicon, which generate low-energy X-rays.

TEM specimens were prepared using a technique similar to that described previously [6] (Fig. 1). A 1 to 2 mm thick slice was cut from the cured material using a low-speed diamond saw, followed by cleaning in acetone. Discs of 3 mm were machined from this slice, using an ultrasonic disc cutter. The discs were mechanically polished, from both sides, to a thickness of 150 to 250 μm. Specimens were dimpled, on one side, down to a central thickness of about 70 μm, using 0.25 μm diamond paste. The other side was then dimpled until a small hole appeared. Specimens were thoroughly rinsed in acetone, followed by rinsing in ethanol, and then bonded to copper rings, for durability and support, with a two-part rapid-setting epoxy. Specimens were ion milled for 1.5 to 2 h, using argon as the sputtering species, at a potential of 4.7 kV, a current of $\approx$ 0.5 mA/gun and an incidence angle of 18° to the horizontal. Carbon-coated specimens were then examined in an Hitachi H-600, 100 kV TEM/STEM equipped with a Kevex beryllium window X-ray detector.

3. Results and discussion

Residual unhydrated clinker was detected in all cement samples. Alite (impure C_3S*) was identified by both X-ray diffraction and TEM/STEM (Fig. 2). Alite is a major constituent of OPC clinker, making up about 55% by weight of the clinker material. Alite, in all cases, appeared in the monoclinic M1-type structure, with lattice parameters; $a = 3.308$ nm, $b = 0.707$ nm, $c = 1.856$ nm and $\beta = 94.17°$. The intense reflections in the selected-area diffraction pattern (SAD) of Fig. 2

*Cement chemistry notation: C = CaO, S = SiO_2, A = Al_2O_3, F = Fe_2O_3, H = H_2O, $\bar{S}$ = SO_3.

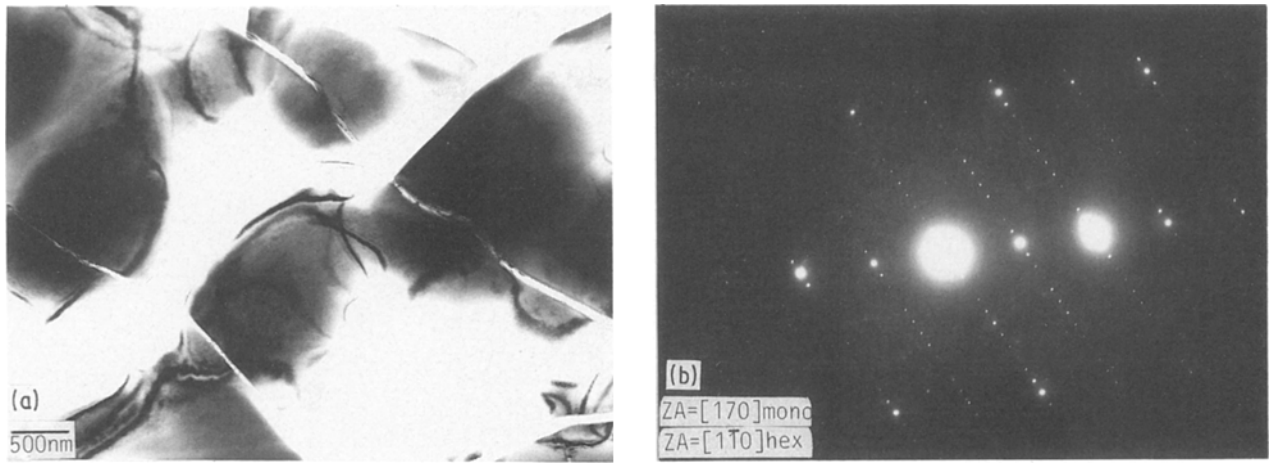

Figure 2 (a) Bright-field micrograph and (b) SAD pattern of a region of unreacted alite in 1.0M Cr cement paste. The beam directions for both the monoclinic and hexagonal cells are given.

arise from the Jeffrey rhombohedral pseudostructure, with hexagonal axes of $a = 0.7\,\text{nm}$ and $c = 2.50\,\text{nm}$. The less intense reflections are from the monoclinic structure.

Free lime or calcia (CaO) (Fig 3) was also detected and its presence was presumably due to incomplete burning during clinker processing. Note, that the region of calcia shown in Fig 3, has partially reacted in the presence of air (specifically CO_2), to form calcite ($CaCO_3$):

$$CaO + CO_2 \rightarrow CaCO_3 \quad \Delta H_f = -178\,\text{kJ mol}^{-1} \quad (1)$$

Chromium was detected in all three concentrations of chromium-containing cement. The major difference between the three concentrations was the frequency of occurrence of chromium. Consequently, we focused our efforts on the 1M Cr concentration, to increase the likelihood of finding chromium.

SEM analysis indicated differences in the gross microstructure between the control and chromium-containing specimens. The major difference between the two types of specimens was the absence of ettringite or any of the AFt ($Al_2O_3 \cdot Fe_2O_3 \cdot$trisulphate) phases in the chromium-containing cement paste (Fig. 4). Chromium appeared to inhibit the formation of ettringite, which may be related to its role as a hydration accelerator. Gypsum, a known retarding additive, is believed to promote ettringite formation [7]. Ettringite hinders the formation of an alumina–silica gel, which is responsible for the initial rapid set. Chromium, being an accelerator, may operate in the opposite way. Note, also, in Fig. 4 the presence of the two major products of hydration, i.e. calcium–silicate–hydrate (C–S–H) and calcium hydroxide (CH).

Chromium was detected virtually everywhere in all the SEM samples. The levels of chromium were quite variable as indicated in the back-scattered electron (BSE) image and accompanying X-ray spectra in Fig. 5. There appears to be a correlation between the silicon and chromium concentrations in the cement paste. As the chromium content increases, the silicon content decreases, indicating that chromium may have substituted for silicon. Further evidence for this was found in the TEM/STEM analysis, which will be discussed in the following paragraphs. Individual phase compositions were difficult to determine because of marked electron beam spreading in the bulk SEM specimens. This problem was not a factor in the TEM/STEM analysis due to the thin nature (100 nm) of the specimens.

Analysis in the TEM/STEM provided a much more detailed, although less statistically representative, view of the hydrated cement paste. All of the major hydration products, with the exception of ettringite

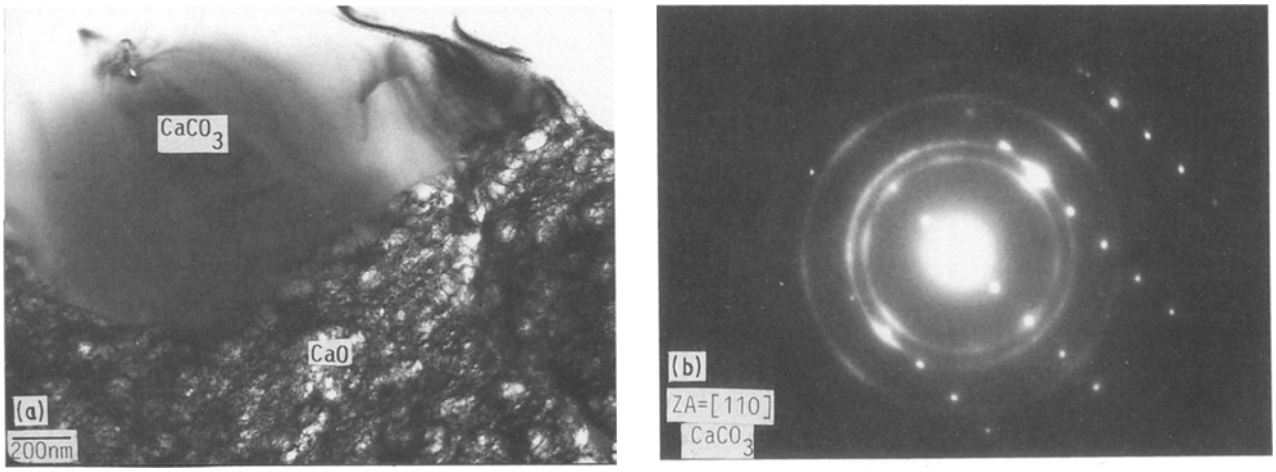

Figure 3 (a) Bright-field image and (b) SAD pattern of region of calcia that has partially reacted to form calcite. The spot pattern in (b) is from the single-crystal calcite, while the ring pattern is from the fcc calcia phase.

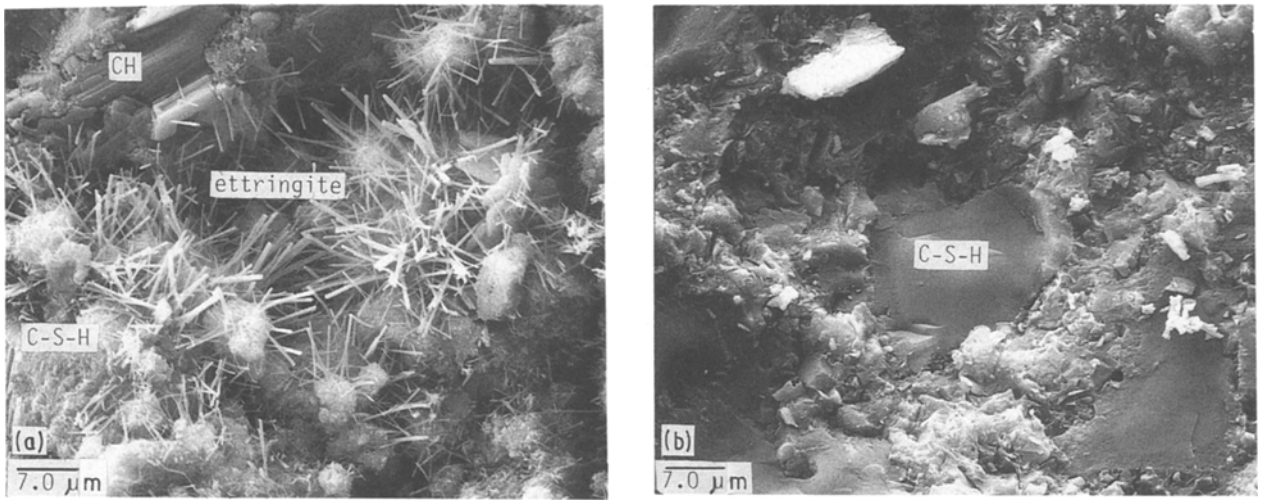

Figure 4 Scanning micrographs of cement paste specimens: (a) control specimen and (b) 1.0M Cr specimen. Note, the presence of ettringite needles in (a) and the absence of ettringite in (b).

(AFt phases), were observed in both the control and chromium-containing cement samples. These are listed in Table II. Chromium was detected in virtually all the hydration products, although not in all instances. The amount of chromium, relative to calcium and silicon, was quite variable, echoing the SEM results.

C–S–H and CH were the most frequently detected phases in the control and chromium-containing specimens. CH, as well as calcite, were detected by X-ray diffraction. Calcite formation arises, in addition to the process discussed above, through the reaction of unprotected CH in the presence of air.

$$Ca(OH)_2 + CO_2 \rightarrow CaCO_3 + H_2O$$
$$\Delta H_f = -69\,kJ\,mol^{-1} \quad (2)$$

A region of C–S–H and CH is shown in Fig. 6, together with accompanying SAD patterns. Both phases contain chromium, although the CH has a significantly higher chromium concentration. Other regions of C–S–H, with much higher levels of chromium, were also observed. An example is shown in Fig. 7, where the accompanying X-ray spectra also demonstrate the wide variability in phase composition. There appears to be a correlation between the chromium and silicon ratios, as mentioned previously in the SEM results. A decrease in the silicon content appeared to be associated with a corresponding increase in chromium content. If this was indeed the case, then the Ca/(Si + Cr) ratios should have approximated the Ca/Si ratios in non-chromium containing cements. Ca/(Si + Cr) ratios were calculated for a limited number of C–S–H regions using a Cliff–Lorimar analysis [8].

For a thin foil specimen the ratio of concentration of two elements is simply proportional to the ratios of the X-ray intensities, i.e.

$$C_A/C_B = k_{A/B} I_A/I_B \quad (3)$$

where C_A and C_B are the concentrations in (wt %) of elements A and B, I_A and I_B are the respective X-ray intensities and $k_{A/B}$ is the proportionality or Cliff–Lorimar factor. The ratios were determined using

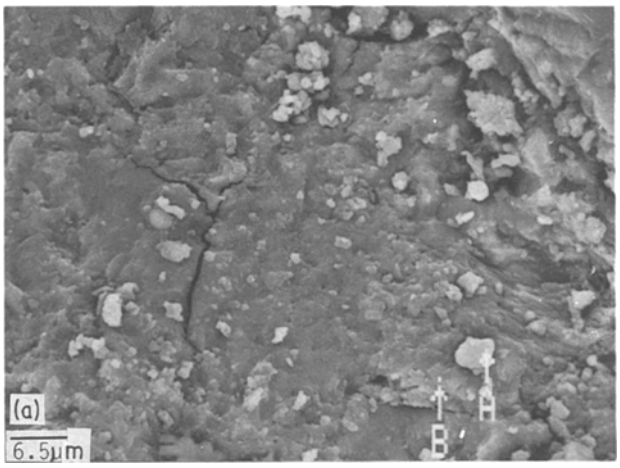

Figure 5 (a) BSE image of a region of 1.0M Cr cement paste. (b, c) X-ray spectra corresponding to regions marked (b) A and (c) B in (a). Note, the apparent inverse relationship between silicon and chromium.

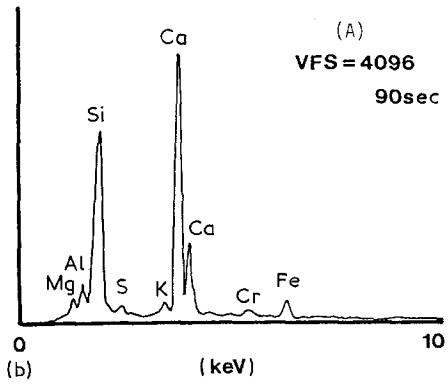

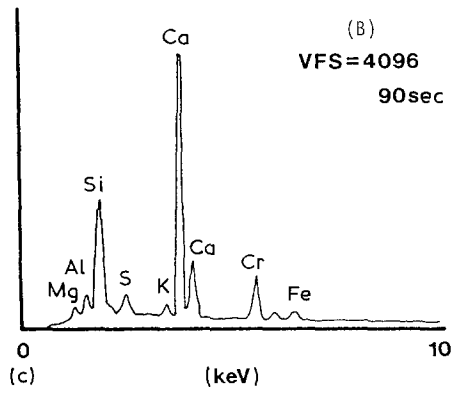

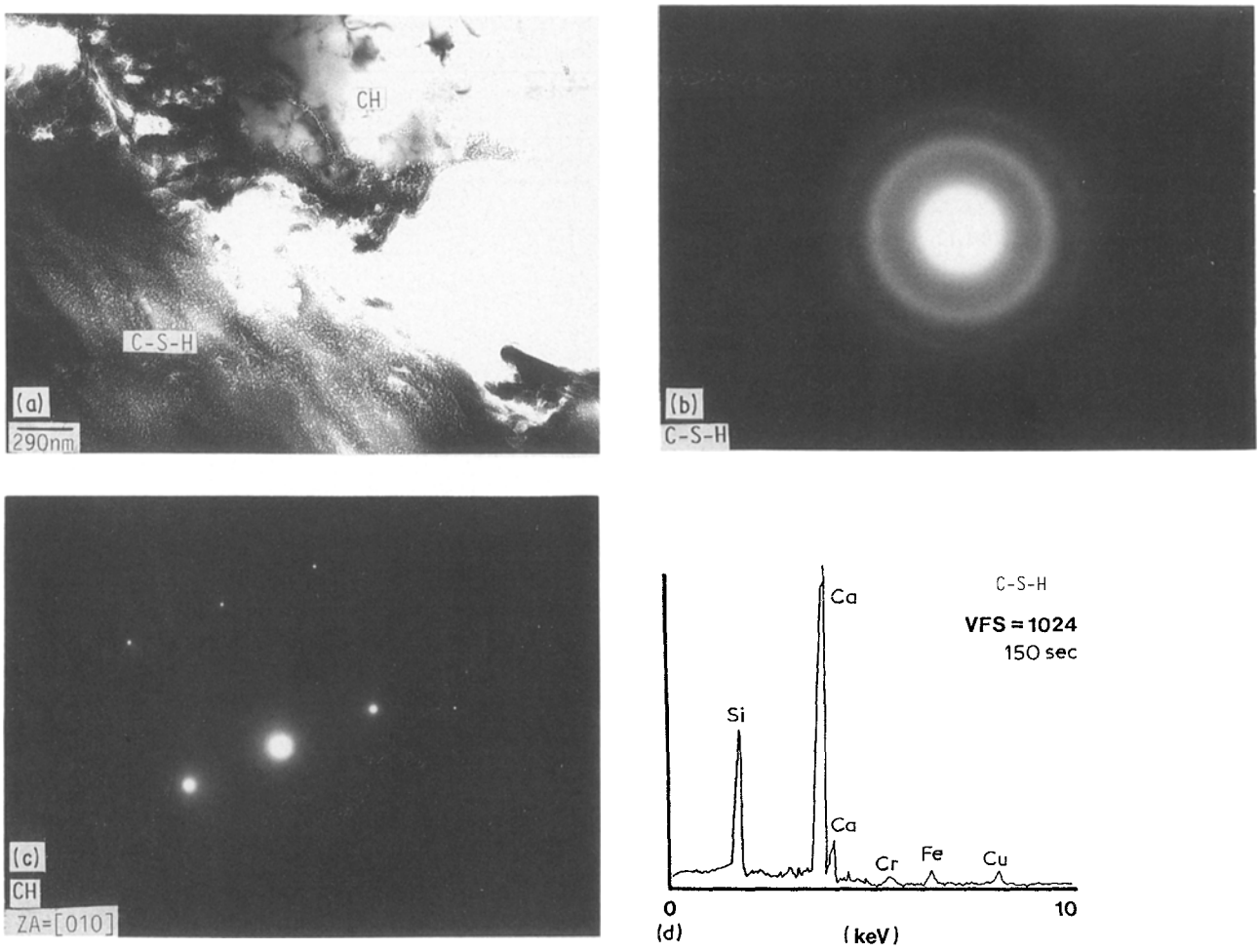

Figure 6 (a) Bright-field micrograph, (b, c) SAD patterns and (d, e) X-ray spectra of a 1.0 M Cr cement paste, showing areas of C–S–H and CH. Both phases contain chromium.

calculated k factors [8] and the results are shown in Table III.

The means and variances of the two test samples were compared to establish whether they belonged to the same population. The sample means were compared using a t-test at a 10% significance level, while the variances were compared by means of an F-test at a 5% level of significance. Neither the variances nor the means were found to vary significantly for these levels of significance, and as such, one can conclude within the degree of confidence stated that the two test samples in Table III belong to the same population, i.e. the assumption is supported that chromium can exchange for silicon in the C–S–H structure.

A possible explanation for the above observations would be the substitution of chromium for silicon in the silicate ions, through the formation of chromate ions (CrO_4^{5-}). There is a charge imbalance, however, as chromium is trivalent and silicon is tretravalent. This imbalance may be offset by the presence of other ions. For example, a hydrogen ion or a hydrated proton H_3O^+ may be associated with each substituted chromium. Other ions such as S^{6+} and Mg^{2+} may be involved, in a more complex manner, as well. The ionic radius ratio of Cr/O is favourable for either tetrahedral or octahedral co-ordination according to Pauling's rules [9], which provides further evidence that chromate ion formation is indeed possible. Cr^{3+} substitution into C–S–H has been reported previously [10, 11]. Tashiro and co-workers [10, 11] have reported that 10% or more of Cr_2O_3 can enter into solid solution with C–S–H. They, however, suggested that Cr^{3+} substitutes for both Ca^{2+} and Si^{4+}, i.e. $2Cr^{3+} = Ca^{2+} + Si^{4+}$. We do not discount this possibility, as our results at this time are somewhat limited. A much more detailed analysis of the Cr^{3+}-substituted C–S–H phase, using k factors

TABLE II Typical hydration products in OPC

Compound	(%)
Calcium silicate hydrate $3CaO \cdot 2SiO_2 \cdot 4H_2O$ (C–S–H)*	60–70
Calcium hydroxide CH	20–30
Al_2O_3–Fe_2O_3–trisulphate AFt	balance
Al_2O_3–Fe_2O_3–monosulphate AFm	balance

*C–S–H variable composition.

determined from standards, is necessary for clarification.

Hydration products of C_3A and C_4AF were also detected, although much more infrequently than C–S–H or CH. In agreement with the earlier SEM results, only the monosulphates (AFm) and not the trisulphates (AFt) were observed. Significant amounts of chromium were detected in these phases. It is likely that chromium substituted for both aluminium and iron, because the ionic charges are the same (3+) and the ionic sizes are comparable.

From a microstructural point of view (TEM/STEM), the waste specimens were very similar to the control specimens. There were, however, two additional phases (other than the normal hydration products) present in the waste samples. One of these phases was polycrystalline and Ca–Cr-rich (Fig. 8). This phase was quite prevalent, i.e. more so than the monosulphate phases. Once again, the composition was quite variable, with a maximum Cr/Ca ratio of ≈ 0.85 (X-ray spectra in Fig. 8). Other elements present in this phase, included silicon, iron and sulphur. We have been unable, at this time, to identify this phase, mainly because of the wide compositional variability.

The other phase, shown in Fig. 9, was only observed in one sample. It was single crystal, as indicated in the convergent-beam electron diffraction (CBED) pattern in Fig. 9. The diffraction pattern matched the crystal structure of $Ca(NO_3)_2$. Chromium, as well as other impurities such as silicon, iron and sulphur, were also present.

From the preceding results, it appears that Cr^{3+} is chemically contained within the cement structure.

TABLE III Composition ratios for C–S–H regions of waste-containing and control cement samples

Chromium-containing regions		Non-chromium-containing regions	
Region	Ca/(Si + Cr) (at %)	Region	Ca/Si (at %)
1	1.2	1	1.2
2	0.6	2	1.2
3	0.6	3	1.2
4	1.3	4	0.6
5	0.7	5	1.9
6	1.2	6	1.6
7	1.2	7	1.9
8	1.2		
9	1.4	mean =	1.41
10	1.1	S.D. =	0.46
11	1.7		
12	1.6		
13	1.8		
14	2.8		
15	3.8		
16	2.1		
17	1.9		
18	2.2		
19	2.1		
20	1.7		
21	2.7		
22	1.9		
23	0.9		
24	2.2		
25	3.0		
mean =	1.72		
S.D. =	0.79		

This appears to be a feature of accelerating additives, whereas retarders tend not to be chemically contained. Lead (Pb^{2+}), for example, is a known hydration retarder and has been found, by photoelectron spectroscopy, to be primarily a surface species in cement paste [12]. This is in contrast to chromium, which, in the same study was barely detectable at the surface. Also, zinc greatly retards hydration of OPC (and pulverized fuel ash, PFA) by performing a layer of amorphous gel on particles with concomitant promotion of ettringite formation that results in a drastic increase in pore volume and the proportion of pores with large radii [13]. Retarders form insoluble salts

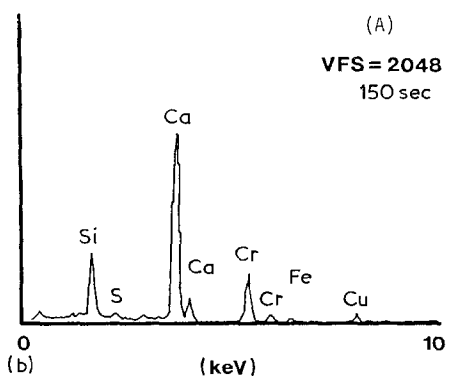

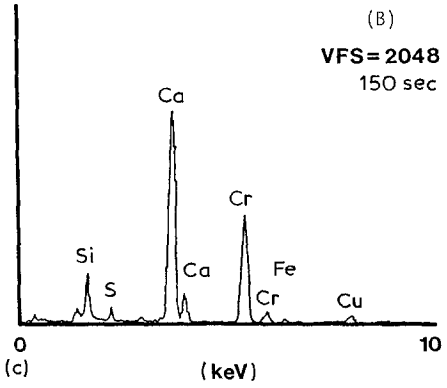

Figure 7 (a) Bright-field micrograph and (b, c) X-ray spectra of a high chromium region of C–S–H in a 1.0 M Cr cement paste. Note, from the X-ray spectra in (b and c), that chromium appears to substitute for silicon.

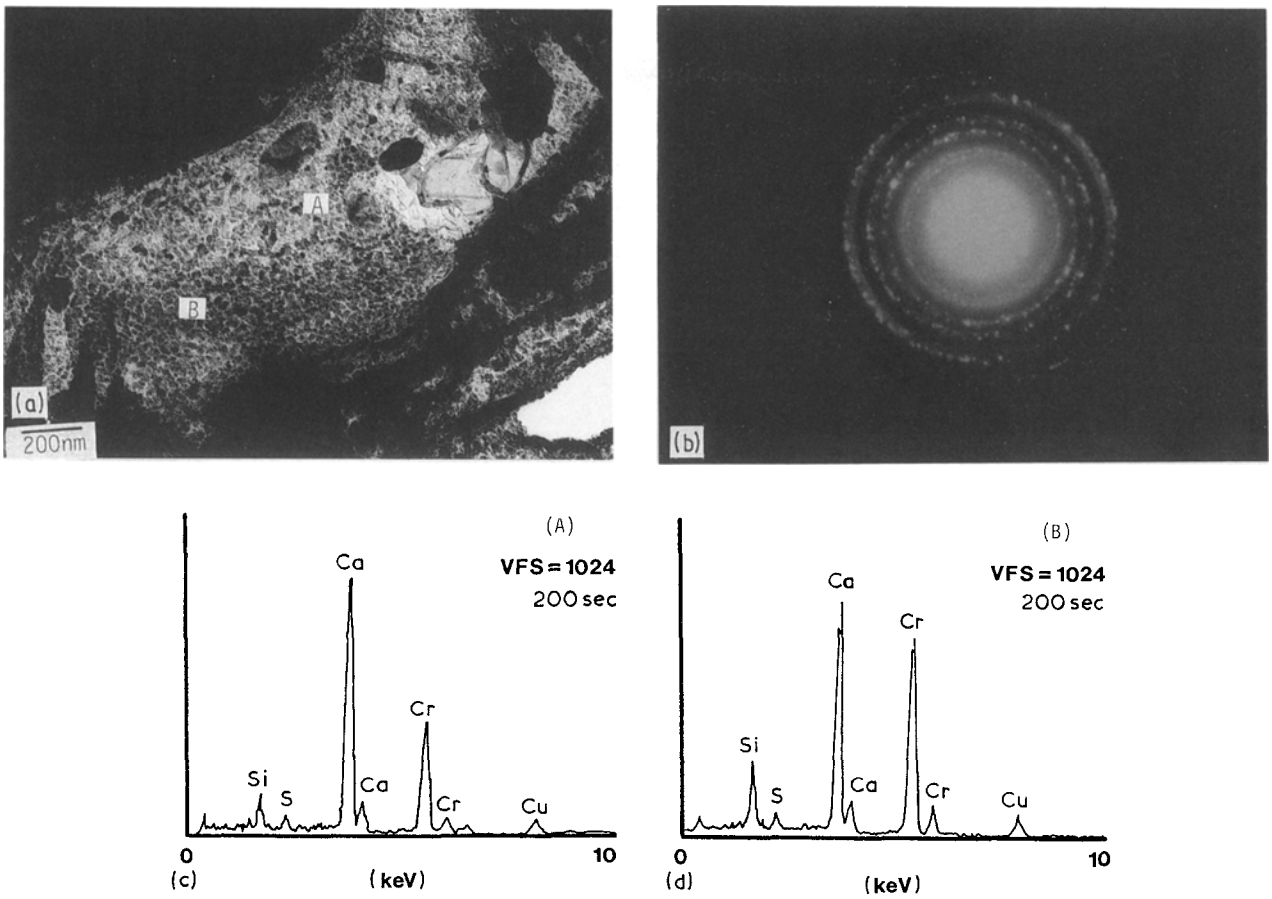

Figure 8 (a) Bright-field image, (b) SAD pattern and (c, d) X-ray spectra from a polycrystalline Ca–Cr-rich region.

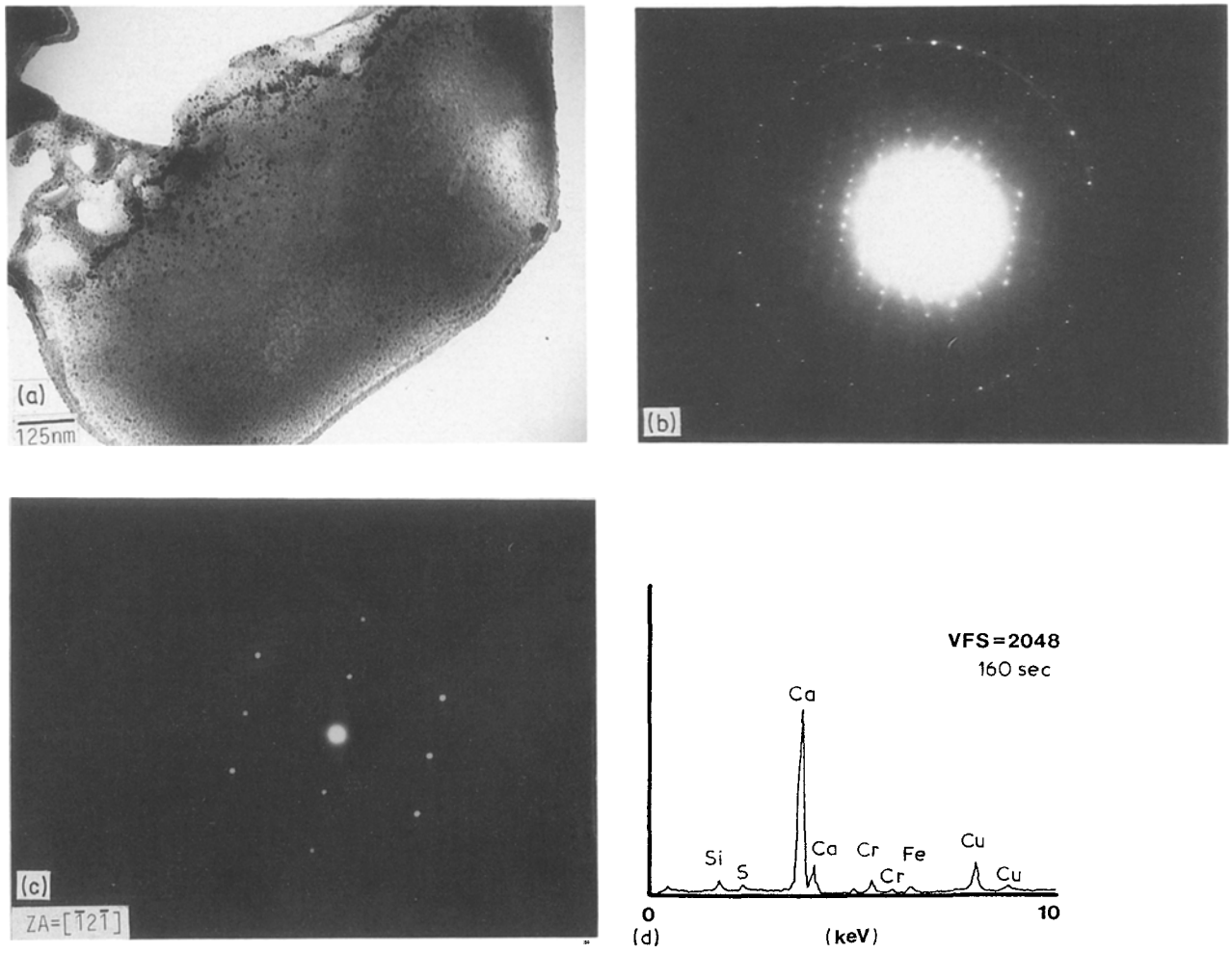

Figure 9 (a) Bright-field image, (b, c) C BED patterns and (d) X-ray spectrum of a region of chromium-containing $Ca(NO_3)_2$.

and tend to precipitate as dense coatings on the hydrating phases [4, 12]. This results in a loss of permeability, effectively forming a diffusion barrier to water. The net result is to slow the rate of hydration. Accelerators, such as chromium, have soluble calcium salts and thus are more easily incorporated into the hydration products.

4. Conclusions

1. Chromium (Cr^{3+}) was chemically incorporated into all phases of hydrated ordinary Portland cement.

2. Chromium appeared to suppress ettringite formation in OPC.

3. Chromium appeared to substitute for silicon in C–S–H and is associated with calcium salts, i.e. $Ca(OH)_2$ and $Ca(NO_3)_2$.

4. Chromium was also detected in polycrystalline Ca–Cr-rich phases, with Cr/Ca ratios as high as 0.85.

References

1. C. S. POON, C. J. PETERS and R. PERRY, *Sci. Total Environ.* **41** (1985) 55.
2. C. S. POON, A. I. CLARK, C. J. PETERS and R. PERRY, *Waste Manag. Res.* **3** (1985) 127.
3. M. NEUWIRTH, R. MIKULA and P. HANNAK, *ASTM STP 1033* edited by T. M. Gilliam and P. Cote (American Society for Testing and Materials, Philadelphia, 1989).
4. N. L. THOMAS, *J. Mater. Sci.* **22** (1987) 3328.
5. J. F. YOUNG (ed), "Cement Research Progress 1981" (American Ceramic Society, 1982).
6. D. G. IVEY and M. NEUWIRTH, *Cem. Concr. Res.* **19** (1989) 642.
7. H. C. EATON, M. B. WALSH, M. E. TITTLEBAUM, F. K. CARTLEDGE and D. CHALASANI, "Microscopic Characterization of Solidification/Stabilization of Organic Hazardous Wastes," presented at "Energy Sources and Technology Conference and Exhibition," Dallas, Texas, 17 to 21 February 1985. ASME 85-Pet-4.
8. J. I. GOLDSTEIN, D. B. WILLIAMS and G. CLIFF, "Quantitative X-ray Analysis," in "Principles of Analytical Electron Microscopy," edited by D. C. Joy, A. D. Romig and J. I. Goldstein (Plenum Press, New York, 1986) p. 155.
9. W. D. KINGERY, "Introduction to Ceramics" (Wiley, New York, 1960).
10. C. TASHIRO and K. KAWAGUCHI, *Cem. Concr. Res.* **7** (1977) 69.
11. C. TASHIRO, H. TAKAHASHI, M. KANAYA, I. HIRAKIDA and R. YOSHIDA, *ibid.* **7** (1977) 283.
12. D. COCKE, J. D. ORTEGO, H. McWHINNEY, K. LEE and S. SHUKLA, *ibid.* **19** (1989) 156.
13. C. S. POON and R. PERRY, *Mater. Res. Soc. Symp. Proc.* **86** (1987) 67.

Received 21 July
and accepted 22 November 1989